MRS Advances (2024) 9:51–56
https://doi.org/10.1557/s43580-023-00622-1

ORIGINAL PAPER

Structural phases of sodium titanate nanotubes obtained in different synthesis conditions: A theoretical study

Lucía Amy[1] · Sofía Favre[1] · Lucía Campo Schneider[2] · Ricardo Faccio[3]

Received: 31 May 2023 / Accepted: 17 July 2023 / Published online: 3 August 2023

Abstract

Sodium-based titanate nanotubes are promising materials for energy applications, declared as one of the ten emerging technologies in chemistry. However, their structural properties, the presence of structural water, and the emergence of mixed phases due to the interchange between *H* and *Na*, are strongly dependent on the synthesis conditions, being difficult to determine the internal structure of these materials. The present work is a theoretical approach based on ab initio calculations to understand the inner structure (building blocks) of the nanotubes. We use as possible models of crystalline structure: hexa ($Na_xH_{2-x}Ti_6O_{13}$) and tri ($Na_xH_{2-x}Ti_3O_7$) titanates of hydrogen and sodium ($x = 0, 1, 2$), suggested by the results of an annealing process on real samples. We calculated the structural, vibrational and electronic properties of the systems under study, founding good agreement with the experiments, thus suggesting the possible coexistence of $Na_xH_{2-x}Ti_3O_7$ and $Na_xH_{2-x}Ti_6O_{13}$ phases in the nanostructured samples.

Introduction

Sodium ion-based technologies for device manufacture or energy storage applications are currently one of the most studied subjects [1]. In particular, nanostructured sodium titanates (NaTNT) are being analyzed as a promising material for the batteries anode development [2–6]. Due to the relevant application of these materials, it is important to have a precise characterization of them. So far there are many studies in the literature trying to elucidate the formation mechanisms and the structural phases of these compounds [1, 7–12]. One strategy is to simulate bulk initial structures, and then calculate the X-ray powder diffraction (XRPDs) for a slab or a rolled slab as a nanotube. With these simulated XRPD patterns, the goal is to fit the experimental diffraction patterns. If both agree, the initial structure can be validated [8].

In previous works [13, 14], we have synthesized this type of materials by the hydrothermal method, varying the synthesis conditions (reaction temperature, reaction time and pH of the medium where the reaction is carried out). Since the final structure influences the optical and electrical properties, it is important to have the former regulated and characterized, to apply these materials in useful devices. This motivates understanding which are the main structural blocks that could build these nanotubes. In [13, 14] we have found that there is not a single crystalline phase that can explain the whole XRPD patterns of these compounds and that the ratio between these phases is affected by the initial conditions of the synthesis. Phases such as di-titanates $Na_2Ti_2O_5$, $Na_2Ti_2O_2H_2O$ (with and without structural water) were analyzed theoretically, as they were suggested by extended X-ray absorption fine structure (EXAFS) experiments [13]. Still, it was not possible to reproduce the experimental diffraction patterns with the simulated ones (see Fig. 1 in Supplementary Material). We proposed that the phases of the compounds are probably tri-titanates of hydrogen and

✉ Sofía Favre
sfavre@fing.edu.uy

Lucía Amy
lamy@fing.edu.uy

Lucía Campo Schneider
lucia.campo@uni-saarland.de

Ricardo Faccio
rfaccio@fq.edu.uy

[1] Instituto de Física, Facultad de Ingeniería, Universidad de la República, Herrera y Reissig 565, 11000 Montevideo, Uruguay

[2] Department of Materials Science and Engineer, Saarland University, Campus D3 3, 66123 Saarbrücken, Germany

[3] Área Física and Centro NanoMat, DETEMA, Facultad de Química, Universidad de la República, Av. Gral. Flores 2124, CC 1157, 11800 Montevideo, Uruguay

sodium with structural water $Na_xH_{2-x}Ti_3O_7 \cdot nH_2O$ following Morgado analysis [10, 11, 14]. Once again, although the tri-titanate phases fit better than Ti_2O_5 phase, they fail to represent faithfully the XRPDs.

Continuing with the efforts of determining the main structural building blocks, we include an extra phase $Na_xH_{2-x}Ti_6O_{13}$. This phase, which was already suggested in the literature after studying the transformation of samples at high-temperature [15–17], was attributed to the transformation of the $Na_xH_{2-x}Ti_3O_7$ phase when all the structural water and H content evaporates.

In this work, we present First Principles based simulations carried out on $Na_xH_{2-x}Ti_3O_7$ and $Na_xH_{2-x}Ti_6O_{13}$ with $x = 0, 1$ and 2 for each phase. With the results of the simulations, the slab XRPD patterns and the bulk off-resonance Raman spectra are evaluated and compared with the experimental ones. The electronic properties are also studied from the density of the electronic states of the systems, from which the bandgap was estimated with two functional. Moreover, the optical absorbance was calculated and compared with experimental measurements.

Materials and methods

Computational method

The ab initio calculations based on density functional theory (DFT) [18, 19] were applied using the Vienna ab initio simulation package (VASP) [20]. This methodology utilizes plane waves as a basis set, with pseudopotentials, incorporating the projector augmented wave method [21]. The selected exchange-correlation functional corresponds to GGA in the Perdew–Burke–Ernzerohf (PBE) [22, 23] parametrization. The basis set was expanded up to an energy cut-off of 400 eV, and the Monkhorst-Pack grid was adjusted to a $4 \times 4 \times 2$. The initial structures were obtained from early reported sodium-based titanates of the following stoichiometry: $Na_2Ti_3O_7$ and $Na_2Ti_6O_{13}$. In order to obtain the corresponding hydrogen-based titanates, we substituted the Na atoms with H atoms: $Na_xH_{2-x}Ti_3O_7$ and $Na_xH_{2-x}Ti_6O_{13}$ for $x = 0, 1$ and 2. These initial structures, including unit cell parameters and atom positions, were fully relaxed with a force tolerance of 0.01 eV/Å and a stress tensor component lower than 1 kBar. Due to the limitations of conventional xc-functionals in DFT, after the full relaxation, we applied the HSE06 screened hybrid functional [24] to get a better description of energy bandgaps. In order to confirm the local stability of the obtained structural geometries, we proceed with the analysis of the phonon spectra utilizing density function perturbation theory (DFPT) [25–28] as implemented in the VASP code. Finally, we simulate the off-resonance Raman spectra of the studied titanates, applying the methodology reported by Porezag et. al. [29], as implemented in the *vasp_raman.py* script (https://github.com/raman-sc/VASP/).

Sample preparation and structural characterization

Nanostructured titanates were synthesized by hydrothermal method under different temperatures, time and pH conditions as reported in [13, 14]. An exhaustive study of its structural, vibrational, and electronic properties has been also published in the previous references. In search of new possible phases that form the obtained nanostructures, an annealing process was performed in a selection of samples in vacuum at 800 °C, after which X-ray scans were performed with a PANanlytical X'Pert MPD X-ray diffractometer. The system was operated with Cu radiation at 40 kV and 40 mA, with a solid-state X-ray detector (PIXcel 1D). The measurements were done at room temperature, mounting a graded parabolic parallel beam X-Ray mirror for Cu-radiation in the incident path and parallel plate collimator in the diffracted path. The measurement range was from 5.00° to 80.00°, with a step size of 0.013° and a counting time of 4.4 s (detector in receiving slit mode).

The conditions for the X-ray diffraction measurement of the samples in the nanostructured state (prior to the annealing process), the Raman spectroscopy spectra and the absorbance coefficient were explained in [13, 14]. When comparing numerical results with experiments, the more relevant hydrothermal conditions are displayed, the rest can be found in the preceding references.

Results

Models: $Na_xH_{2-x}Ti_3O_7$ and $Na_xH_{2-x}Ti_6O_{13}$, x = 0,1 and 2

As mentioned in the "Sample preparation and structural characterization" section, a selection of the previously reported samples underwent an annealing process. The XRPDs after the annealing process are presented in Fig. 1a. The final phases were identified with sodium tri-titanates $Na_2Ti_3O_7$ and hexa-titanates $Na_2Ti_6O_{13}$, in different proportions depending on the synthesis condition. In the literature, the hexa-titanate phase usually appears as a derivative of the dehydrated tri-titanate phase [15–17]. However, there is no evidence to rule out the possibility that the hexa-titanate phase is prior to the annealing process. For this reason, six possible starting structures are simulated, taking $Na_2Ti_3O_7$ and $Na_2Ti_6O_{13}$ as the starting structures, and replacing Na with H, partially and totally. The models used are shown in Fig. 1b.

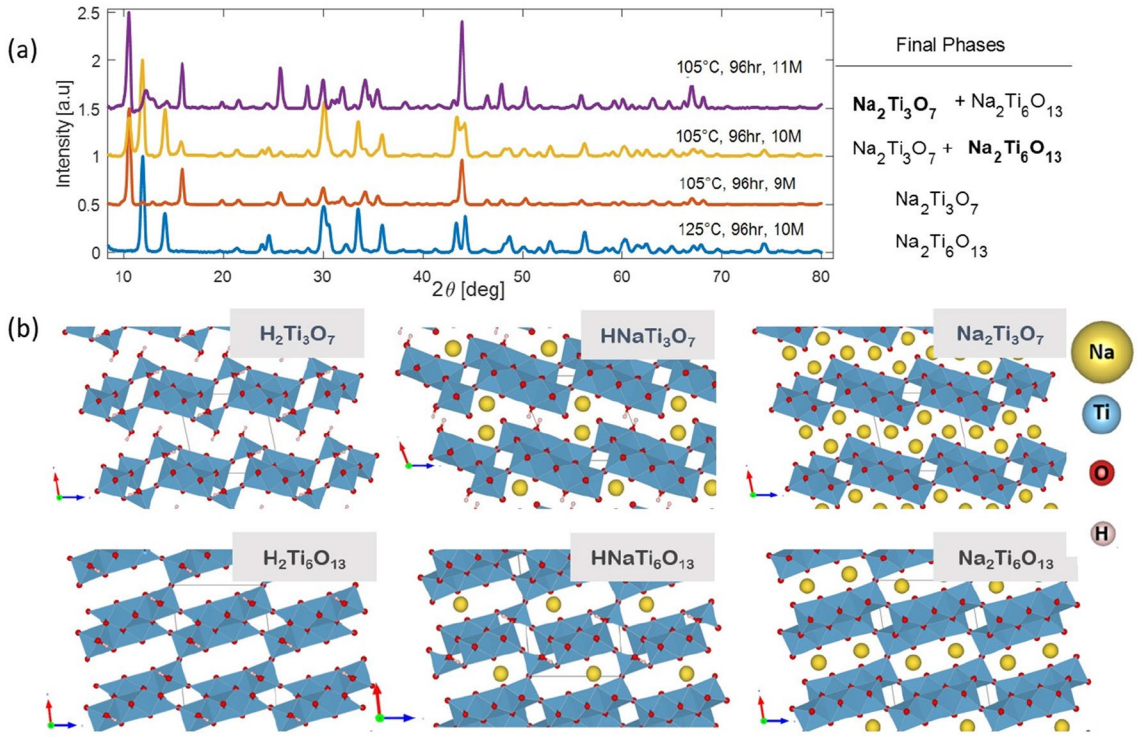

Fig. 1 **a** Standard $\theta - 2\theta$ XRPD scans for NaTNT samples after the annealing process at 800 °C; **b** Structural models for possible starting phases

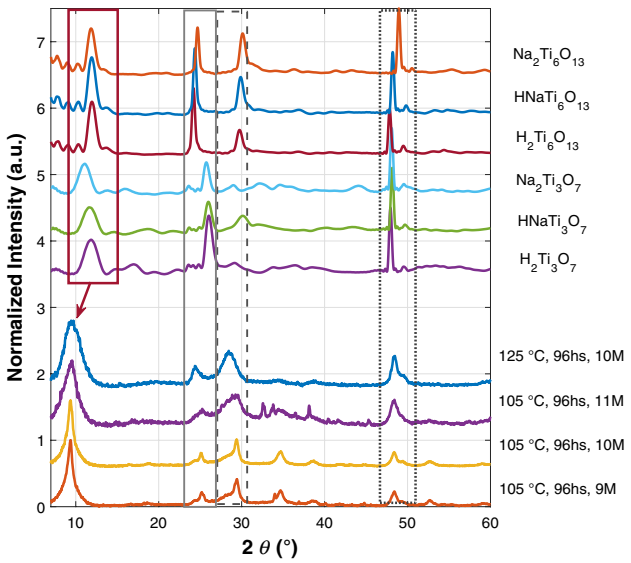

Fig. 2 XRPD spectra for four samples (with the hydrothermal conditions in the figure), and simulated XRPD diffraction for the six building block considering a slab enrolled with a periodicity of 6*a* radial, 50*b* axial and 8*c* tangential

Structural properties: XRPD and Raman

Figure 2 shows the diffraction patterns for a selection of four samples manufactured by the hydrothermal method [14] compared with the XRPD obtained for the six models considered. It is observed that the correspondence is not univocal, but this is to be expected since the simulated patterns correspond to slab enrolled with a certain periodicity, and the mixture of them was not evaluated. However, we found great similarities between the patterns. For example, the peaks at $2\theta \sim 9.5°$ and $2\theta \sim 48 - 50°$ appear in all cases. The position of the first one is associated to the distance between sheets and its width is related to the wall of the nanotube. The difference in positions can be explained with the lack of structural water in the theoretical models. This water would be located between sheets, increasing the radial lattice parameter, and thereby decreasing the position of the diffraction peak. This was confirmed by measuring the diffraction pattern under vacuum, where the elimination of water generates an appreciable shift of the mentioned peak (see Fig 4. in Supplementary Material). The peak at $2\theta \sim 48 - 50°$ is obtained in the correct position. The presence of the both phases (tri and hexa) is necessary to explain the peaks doublets in the region between $2\theta \sim 23 - 30°$, since a mixture of only *H* and *Na* in the same phase would not be enough to explain its separation.

Experimental and simulated Raman spectra are shown in Fig. 3, for the same samples and simulated structures. Again, similarities are observed between the simulated and experimental Raman bands, where the five most intense and relevant bands were identified. However, due to the

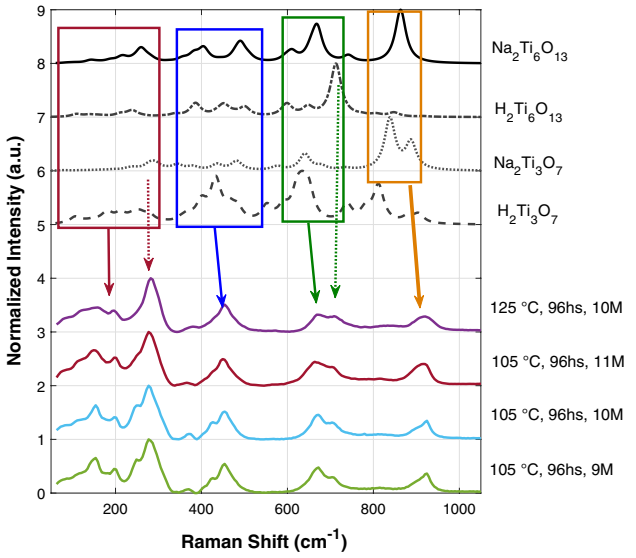

Fig. 3 Raman spectra for four selected samples (with the Hydrothermal conditions in the figure), simulated Raman spectra for the four building block considered in bulk

bulk character of the structure used to simulate the Raman spectra, peaks may change in wide and central peak positions. But taking those effects, and the tendency of DFT in underestimating the simulated frequencies, we can conclude that there is a reasonable agreement. Additionally, and in reference to the correct band's assignment when there is the presence of *Na* atoms, we can generally establish that regions between wave-number $k = 0$ to $350\,\mathrm{cm}^{-1}$ correspond to Na–Ti–O vibrations, then the regions between 350 and $1000\,\mathrm{cm}^{-1}$ correspond to Ti–O vibrations and finally when there is hydrogen atoms present almost free O–H vibrations occur in the region of $3000\,\mathrm{cm}^{-1}$. In the case of samples with *Na* atoms content, the strong signal locate between 800 and $1000\,\mathrm{cm}^{-1}$, comes from the electronic polarizability effects of it cation in the Ti and O atoms close to the inter-lamella or channel cavities for tri- and hexa-titanates structures. When comparing with the experimental measurements, to explain the double peaks in the region 600–$800\,\mathrm{cm}^{-1}$, it again seems necessary to consider both types of phases.

Both structural characterizations were in support of a mixture of phases in the nanostructured samples.

Electronic properties

Electronic structure properties were calculated using conventional xc-functional GGA-PBE and with the HSE06 screened hybrid functional, in order to compare electronic structure results. The electronic density of states looks as expected, showing a semiconductor behavior with a clear separation of the valence—and conduction band with an energy gap around 3 eV. The valence band (BV) is mainly dominated by O-2p states, while Ti-3d states mainly contribute to the conduction band (CB). The contributions from *H* and *Na* states are totally negligible in the region of the Fermi levels, as expected. But their presence introduces changes in the total charge of Ti atoms, which establishes slight changes in the band positions and DOS changes, thus modifying the VB and CB indirectly. The DOS curves and bandsgaps values obtained from them are summarized in the Supplementary Material.

Tri-titanates present higher bandgaps in comparison to hexa-titanates, and an increase in bandgaps is observe when going from $x = 0$ to 2 for both phases. This trend, that was observed priory in the bibliography [11], it is further confirmed by DFT calculations. Here it is important to mention that besides the fact that GGA-PBE underestimates the bandgaps, the correct trend is recovered with this analysis. In order to improve the determination of this electronic structure–property, hybrid HSE06 was also applied, obtaining an overestimation of the bandgap values between 4.3 and 4.8 eV, with the same trends obtained for PBE-GGA. Furthermore, if we consider the hexa-titanate as the high-temperature structure of the tri-titanate, then the expected reduction of the bandgap is also recovered.

Figure 4 shows the calculated optical absorbance for the six structures, and two examples of experimentally measured absorbance. The shapes of optical absorbance spectra for both systems present similarities. It can be highlighted that experimental samples exhibit multiple bandgap edges in absorbance curves. The staggered form also appears in the calculated absorbance. This supports the presence of these phases.

Therefore, the main conclusion here is that conventional HSE06, in terms of relative weights of exchange and correlations, did not properly describe the energy bandgaps of tri and hexa-titanates. It requires further correction, but the single analysis made by GGA-PBE is sufficient to recover the trends and shapes of the optical absorbance properties.

Conclusion

We performed ab initio calculations in order to understand the inner structure of the titanate-based nanotubes, which will help to predict their structural, vibrational, and electronic structure properties. The potential crystalline structure models of hexa ($Na_xH_{2-x}Ti_6O_{13}$) and tri ($Na_xH_{2-x}Ti_3O_7$) titanates, including hydrogen and sodium, suggested by experimental results, demonstrated to be reasonable for the expected description. The calculated XRPD, Raman spectra and optical properties present good correspondence with the experimental data. To explain the peaks doublet that appears in the diffraction patterns for 2θ between 20 and 30°, it is

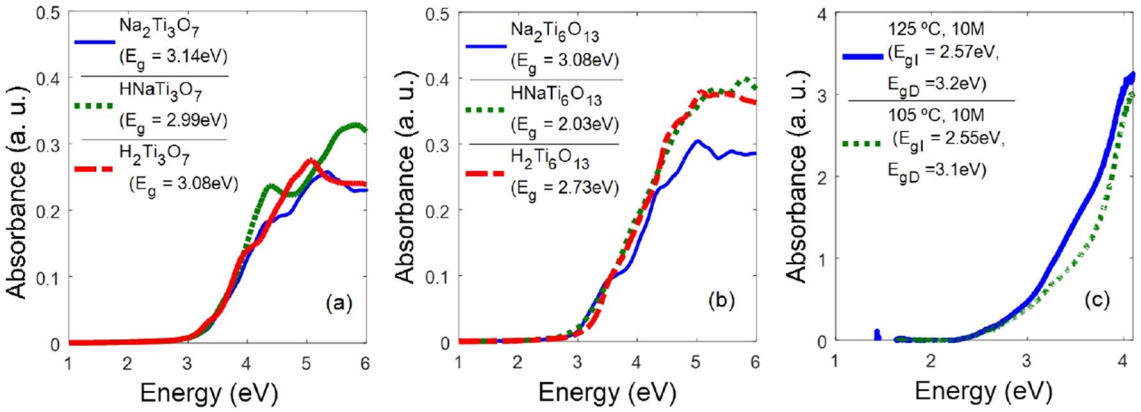

Fig. 4 Simulated absorbance for the structures based on **a** tri-titanates, **b** hexa-titanates, and **c** experimental measurements of absorbance for two synthesis conditions. The insets in the figure show the bandgaps values estimated by DOS and experimentally obtained

necessary to consider both (tri- and hexa- titanate) phases. On the other hand, the level of mixture between *H* and *Na* will help to better predict or explain the position of each contributing peaks. Furthermore, when the sample is synthesized at a higher temperature it appears to have a greater contribution from the hexa-titanate phase. Similarly, there are doublets in the case of Raman spectra that cannot be explained if we do not consider both phases, for example in the bands around the 600–800 cm^{-1} region. This suggests the possible coexistence of these two phases prior to the high temperature annealing process. The bandgap calculations with the PBE functional underestimate the gap but allow to justify variations in the range of 2 to 3.3 eV, as observed in this type of structures. In summary, joint experimental and simulation procedures can give relevant responses to complex systems based on nanostructured systems. Next step would be to refine further the contribution of the different phases.

Supplementary Information The online version contains supplementary material available at https://doi.org/10.1557/s43580-023-00622-1.

Acknowledgments The authors wish to thank the Uruguayan *CSIC*, *ANII* and *PEDECIBA* funding institutions. We also want to thank F. Mücklich for the HT-XRD measurement at the Chair of Functional Materials Department of Material Science, Saarland University, Germany.

Author contributions Authors confirm contribution to the paper as follows: study conception and design: SF, LA, RF; data collection: LA, LC, RF, SF; analysis and interpretation of results: SF, LA, RF; draft manuscript preparation: SF, LA, LC, RF. All authors reviewed the results and approved the final version of the manuscript.

Data availability Not applicable

Code availability Not applicable

Declarations

Conflict of interest The authors have no competing interests to declare that are relevant to the content of this article. The authors have no financial or proprietary interests in any material discussed in this article.

Ethical approval Not applicable

Informed content All the authors are aware of its content and approve to participate.

Consent for publication All the authors are aware of its content and approve its submission.

References

1. S. Reghunath, D. Pinheiro, K.R. Sunaja Devi, A review of hierarchical nanostructures of TiO2: advances and applications. Appl Surf. Sci. Adv. **3**, 100063 (2021). https://doi.org/10.1016/j.apsadv.2021.100063
2. W. Wang, W. Li, S. Wang, Z. Miao, H.K. Liu, S. Chou, Structural design of anode materials for sodium-ion batteries. J. Mater. Chem. A **6**(15), 6183–6205 (2018). https://doi.org/10.1039/C7TA10823K
3. M.D. Slater, D. Kim, E. Lee, C.S. Johnson, Sodium-ion batteries. Adv. Funct. Mater. **23**(8), 947–958 (2013)
4. S.W. Kim, D.H. Seo, X. Ma, G. Ceder, K. Kang, Electrode materials for rechargeable sodium-ion batteries: potential alternatives to current lithium-ion batteries. Adv. Energy Mater. **2**(7), 710–721 (2012). https://doi.org/10.1002/aenm.201200026
5. S. Guo, J. Yi, Y. Sun, H. Zhou, Recent advances in titanium-based electrode materials for stationary sodium-ion batteries. Energy Environ Sci **9**(10), 2978–3006 (2016). https://doi.org/10.1039/C6EE01807F
6. I. Hasa, S. Mariyappan, D. Saurel, P. Adelhelm, A.Y. Koposov, C. Masquelier, L. Croguennec, M. Casas-Cabanas, Challenges of today for Na-based batteries of the future: from materials to cell metrics. J Power Sour **482**, 228872 (2021)
7. S. Dong, N. Lv, Y. Wu, Y. Zhang, G. Zhu, X. Dong, Titanates for sodium-ion storage. Nano Today **42**, 101349 (2022)

8. M. Esteves, L. Fernández-Werner, F. Pignanelli, M. Romero, M.R. Chialanza, R. Faccio, Á.W. Mombrú, A step forward towards the structural characterization of Na2Ti2O5· H2O nanotubes and their correlation with optical and electric transport properties. Ceram. Int. **46**(3), 2877–2886 (2020). https://doi.org/10.1016/j.ceramint.2019.09.281
9. L. Fernández-Werner, F. Pignanelli, B. Montenegro, M. Romero, H. Pardo, R. Faccio, Á.W. Mombrú, Characterization of titanate nanotubes for energy applications. J. Energy Storage **12**, 66–77 (2017). https://doi.org/10.1016/j.est.2017.04.002
10. E. Morgado Jr., M.A. de Abreu, O.R. Pravia, B.A. Marinkovic, P.M. Jardim, F.C. Rizzo, A.S. Araújo, A study on the structure and thermal stability of titanate nanotubes as a function of sodium content. Solid State Sciences. **8**(8), 888–900 (2006). https://doi.org/10.1016/j.solidstatesciences.2006.02.039
11. E. Morgado Jr., P. Jardim, B.A. Marinkovic, F.C. Rizzo, M.A. De Abreu, J.L. Zotin, A.S. Araújo, Multistep structural transition of hydrogen trititanate nanotubes into TiO2-b nanotubes: a comparison study between nanostructured and bulk materials. Nanotechnology. **18**(49), 495710 (2007). https://doi.org/10.1088/0957-4484/18/49/495710
12. J. Xie, X. Wang, Y. Zhou, Understanding formation mechanism of titanate nanowires through hydrothermal treatment of various ti-containing precursors in basic solutions. J. Mater. Sci. Technol. **28**(6), 488–494 (2012). https://doi.org/10.1016/S1005-0302(12)60087-5
13. L. Amy, S. Favre, D.L. Gau, R. Faccio, The effect of morphology on the optical and electrical properties of sodium titanate nanostructures. Appl. Surf. Sci. **555**, 149610 (2021)
14. L. Amy, S. Favre, R. Faccio, Structural, optical, and electrical properties of proton intercalation h+/na+ phases in nanostructured titanates induced by ph during hydrothermal synthesis. Mater. Today Commun. **33**, 104908 (2022)
15. R. Yoshida, Y. Suzuki, S. Yoshikawa, Effects of synthetic conditions and heat-treatment on the structure of partially ion-exchanged titanate nanotubes. Mater. Chem. Phys. **91**(2–3), 409–416 (2005). https://doi.org/10.1016/j.matchemphys.2004.12.010
16. K. Zhu, Y. Yuan, M. Zhang, J. Hong, Y. Deng, Z. Yin, Structural transformation from NaHTi3O7 nanotube to Na2Ti6O13 nanorod. Solid State Commun. **144**(10–11), 450–453 (2007). https://doi.org/10.1016/j.ssc.2007.09.015
17. A.-L. Sauvet, S. Baliteau, C. Lopez, P. Fabry, Synthesis and characterization of sodium titanates Na2Ti3O7 and Na2Ti6O13. J. Solid State Chem. **177**(12), 4508–4515 (2004). https://doi.org/10.1016/j.jssc.2004.09.008
18. P. Hohenberg, W. Kohn, Inhomogeneous electron gas. Phys. Rev. **136**(3B), 864 (1964). https://doi.org/10.1103/PhysRev.136.B864
19. W. Kohn, L.J. Sham, Self-consistent equations including exchange and correlation effects. Phys. Rev. **140**(4A), 1133 (1965). https://doi.org/10.1103/PhysRev.140.A1133
20. G. Kresse, J. Hafner, Ab initio molecular dynamics for liquid metals. Phys. Rev. B **47**(1), 558 (1993). https://doi.org/10.1103/PhysRevB.47.558
21. P.E. Blöchl, Projector augmented-wave method. Phys. Rev. B **50**(24), 17953 (1994). https://doi.org/10.1103/PhysRevB.50.17953
22. J.P. Perdew, K. Burke, M. Ernzerhof, Generalized gradient approximation made simple. Phys. Rev. Lett. **77**(18), 3865 (1996). https://doi.org/10.1103/PhysRevLett.77.3865
23. J.P. Perdew, M. Ernzerhof, K. Burke, Rationale for mixing exact exchange with density functional approximations. J. Chem. Phys. **105**(22), 9982–9985 (1996). https://doi.org/10.1063/1.472933
24. A.V. Krukau, O.A. Vydrov, A.F. Izmaylov, G.E. Scuseria, Influence of the exchange screening parameter on the performance of screened hybrid functionals. J. Chem. Phys. **125**(22), 224106 (2006). https://doi.org/10.1063/1.2404663
25. S. Baroni, P. Giannozzi, A. Testa, Green's-function approach to linear response in solids. Phys. Rev. Lett. **58**(18), 1861 (1987). https://doi.org/10.1103/PhysRevLett.58.1861
26. X. Gonze, Perturbation expansion of variational principles at arbitrary order. Phy. Rev. A **52**(2), 1086 (1995). https://doi.org/10.1103/PhysRevA.52.1086
27. X. Gonze, Adiabatic density-functional perturbation theory. Phys. Rev. A **52**(2), 1096 (1995). https://doi.org/10.1103/PhysRevA.52.1096
28. S. Baroni, S. De Gironcoli, A. Dal Corso, P. Giannozzi, Phonons and related crystal properties from density-functional perturbation theory. Rev. Mod. Phys. **73**(2), 515 (2001). https://doi.org/10.1103/RevModPhys.73.515
29. D. Porezag, M.R. Pederson, Infrared intensities and raman-scattering activities within density-functional theory. Phys. Rev. B **54**(11), 7830 (1996). https://doi.org/10.1103/PhysRevB.54.7830